Vertical Alignments of Graphene Sheets Spatially and Densely Piled for Fast Ion Diffusion in Compact Supercapacitors

Yeoheung Yoon,[†] Keunsik Lee,[‡] Soongeun Kwon,[§] Sohyeon Seo,[‡] Heejoun Yoo,[†] Sungjin Kim,[‡] Yonghun Shin,[†] Younghun Park,[‡] Doyoung Kim,[†] Jae-Young Choi,[∥] and Hyoyoung Lee[†,‡,⊥,*]

[†]National Creative Research Initiative, Center for Smart Molecular Memory, Department of Energy Science, Sungkyunkwan University, 2066 Seoburo, Jangan-Gu, Suwon, Gyeonggi-Do 440-746, Republic of Korea, [‡]Department of Chemistry, Sungkyunkwan University, 2066 Seoburo, Jangan-Gu, Suwon, Gyeonggi-Do 440-746, Republic of Korea, [§]R&D Center, Samsung Corning Precision Materials Co., Ltd., Tanjeong-myeon Asan-city, 336-725, Republic of Korea, [⊥]Samsung-SKKU Graphene Center, SKKU Advanced Institute of Nano Technology (SAINT), Sungkyunkwan University, 2066 Seoburo, Jangan-Gu, Suwon, Gyeonggi-Do 440-746, Republic of Korea, and [∥]Graphene Research Center, Samsung Advanced Institute of Technology (SAIT), Yongin, Gyeonggi-Do 446-712, Republic of Korea. Y.Y. and H.L. designed the research, Y.Y., K.L., S.S., H.J., Y.S., Y.P., and D.K. carried out the experiments, Y.Y., S.K., and J.C. analyzed and interpreted the data, and Y.Y. and H.L. cowrote the manuscript and Supporting Information.

ABSTRACT Supercapacitors with porous carbon structures have high energy storage capacity. However, the porous nature of the carbon electrode, composed mainly of carbon nanotubes (CNTs) and graphene oxide (GO) derivatives, negatively impacts the volumetric electrochemical characteristics of the supercapacitors because of poor packing density (<0.5 g cm^{-3}). Herein, we report a simple method to fabricate highly dense and vertically aligned reduced graphene oxide (VArGO) electrodes involving simple hand-rolling and cutting processes. Because of their vertically aligned and opened-edge graphene structure, VArGO electrodes displayed high packing density and highly efficient volumetric and areal electrochemical characteristics, very fast electrolyte ion diffusion with rectangular CV curves even at a high scan rate (20 V/s), and the highest volumetric capacitance among known rGO electrodes. Surprisingly, even when the film thickness of the VArGO electrode was increased, its volumetric and areal capacitances were maintained.

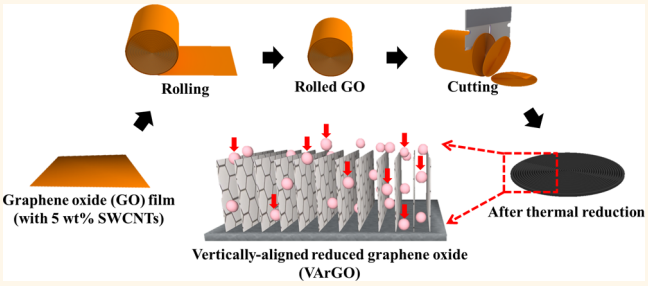

KEYWORDS: vertically aligned · reduced graphene oxide · electrochemistry · supercapacitor

Reduced graphene oxides (rGOs) derived from graphene oxide (GO),[1] called graphene flakes, have been widely studied as carbon-based electrode materials for electrical energy storage (EES) devices such as supercapacitors[2−7] and secondary lithium ion batteries (LIBs)[8−10] because of their high electrical conductivity,[11−13] high surface area,[6,14,15] and good compatibility with polymers and/or metal oxides.[16,17] Non-CDV-grown rGO nanothick sheets are the best materials for EES devices because production of these nanosheets is easy and cheap, enabling mass-production.[18,19] Even though numerous rGO capacitors have been reported,[5,6,8,14] their limited volumetric capacitance has not been addressed, even though this is critical issue for real capacitor applications.[20] Volumetric performance in a limited space is essential if rGO-based ECs are to be used effectively in mobile electronics, electric vehicles, and other compact electronic devices.[20] Until now, however, most researchers have reported high performance supercapacitors based on gravity capacitance measurements, not volumetric capacitance measurements; conversion of gravity capacitance values to volumetric capacitance units yields lower values.[21] In particular, gravity capacitance measurements do not consider the interlayer gap distance between rGO layers, structural uniformity, or the density of rGO nanosheets, while volumetric capacitance measurements reflect packing density in a limited space.[20,21] To realize rGO-based ECs, development

* Address correspondence to hyoyoung@skku.edu.

Received for review January 9, 2014 and accepted March 29, 2014.

Published online March 30, 2014
10.1021/nn500150j

with high volumetric capacitance is an absolute requirement.

A high-performance supercapacitor would ideally have the following characteristics: (1) high packing density of uniformly aligned graphene nanostructures with highly dense graphene sheets to obtain a high volumetric energy density,[21] (2) vertically oriented or aligned graphene nanosheets on the current collector with a suitable pore size and distribution to facilitate high mobility of electrolyte ions,[9,11,22,23] and (3) short paths and ease of access of electrolyte ions to the graphene layers, even in thick films at a high scan rate.[9,11,23] Horizontally aligned carbon electrode materials derived from GOs and carbon nanotubes (CNTs) have been used to achieve a high surface area and suitable pore size.[21,24] However, the packing density reported is still less than 0.5 g cm^{-3}.[20,21,25] Recently, several rGO-derived electrodes with a high packing density such as compressed rGO electrodes[26] and liquid-mediated rGO electrodes[21] have been reported. However, electrolyte ions are not able to diffuse easily through horizontally aligned rGO films because of close stacking of two-dimensional rGO sheets.[9,23,24] This may be because the path lengths of horizontal rGO film are too long, and the interlayer gap distance between rGO layers is too close because of strong pi−pi electron interactions of rGO nanosheets. To overcome these horizontal stacking problems, direct growth of vertically orientated radio frequency plasma-enhanced chemical vapor deposition (RF PECVD)-grown graphene has been reported,[11] but the packing density of the resulting RF PECVD-graphene film with an interlayer distance of a few hundred nanometers was very low. Furthermore, the use of PECVD-graphene as a supercapacitor material is not realistic because of the expensive synthesis process. To create a commercially viable supercapacitor product, easy, cheap, and mass-producible rGO nanosheets would be the best candidate for the electrode materials, and all issues concerning volumetric packing density with an appropriate interlayer rGO gap distance and vertically oriented rGO nanosheets should be addressed simultaneously for the device structure.[21,25] Vertically oriented graphene on the current collector is believed to provide an ideal structure for EC electrodes capable of high frequency operation.[4,11] Therefore, a novel approach to vertically align rGO nanosheets and to control the interlayer gap distance while ensuring high packing density and ease of charging/discharging of electrolyte, even at high scan rates, is required.

Herein, we report a novel method to produce highly dense and vertically aligned rGO (VArGO) involving simple hand rolling and cutting; this approach yielded rGO with a high packing density (1.18 g cm^{-3}) and enhanced electrochemical behavior. As described in the literature,[14,27] GO is in an isotropic phase material and is randomly dispersed in aqueous suspension. As its concentration increases, the isotropic−nematic transition occurs, and fully dried GO sheets begin to align, resulting in the formation of dense, homogeneous, and horizontally stacked GO film.[14,27] As described in Scheme 1, we rolled as-made GO film with a little solvent on its surface to facilitate good adhesion between film surfaces. Then, we cut the rolled GO film at −40 °C using a rotary cryomicrotome before drying (see detailed experimental procedure in the Supporting Information). Freezing of the rolled GO film helped to avoid damage to the cross-section during cutting. When a cut piece of the rolled GO film was placed on a substrate, the GO film was vertically aligned (VAGO), yielding a high packing density of 1.33 g cm^{-3}.

RESULTS AND DISCUSSION

We evaluated various reduction temperatures and heating rates to control the interlayer gap distance between the vertically aligned rGO nanosheets (hereafter referred to as pore size). As described in the literature,[28] reduction of GO starts at below 150 °C; we confirmed this with X-ray diffraction spectroscopy (XRD). The diffraction peak of the rGO film shifted depending on the degree of reduction, which corresponds to the interlayer distance of rGO nanosheets. XRD results revealed a broad diffraction peak at nearly 23° for VArGO treated at 130 °C at a heating rate of 0.14 °C/min (Figure S3, Supporting Information). Only a small and broad diffraction peak at around 12° was detected, indicating that reduction of GO was almost complete at the low temperature of 130 °C. These results indicate that reduction at low temperature allowed a control of the interlayer gap distance (called pore size) of the rGO sheets.[21] For a high temperature at 1000 °C, which is necessary for high conductivity of rGO electrodes, a small amount of single-walled carbon nanotubes (SWCNTs) (less than 5 wt %) was added as a spacer to prevent close stacking of VArGO nanosheets and to maintain a suitable interlayer distance at high temperature, and also to get high conductivity of VArGO.[25,29] As a result, the 21.66° XRD peak of VArGO film that was thermally reduced with SWCNTs (5 wt %) at 1000 °C with the same heating rate was much broader than that of rGO chemically reduced by hydrazine (diffraction peak of 26.22°) and rGO thermally reduced at 1000 °C without SWCNTs (diffraction peak of 26.48°) (Figure S3, Supporting Information). This XRD analysis showed that the VArGO with SWCNTs indicated a nearly amorphous structure in comparison with the others. Only a small and broad peak appeared at 21.66°, corresponding to a d_{002} distance of 0.41 nm; however, the diffraction peak was much weaker and broader than those of the VArGO without SWCNTs and chemically reduced rGO. In addition, diffraction peak in low angle (~10°) emerged, which corresponds to the pore size of around 0.8 nm. Thus, the VArGO sheets did not restack

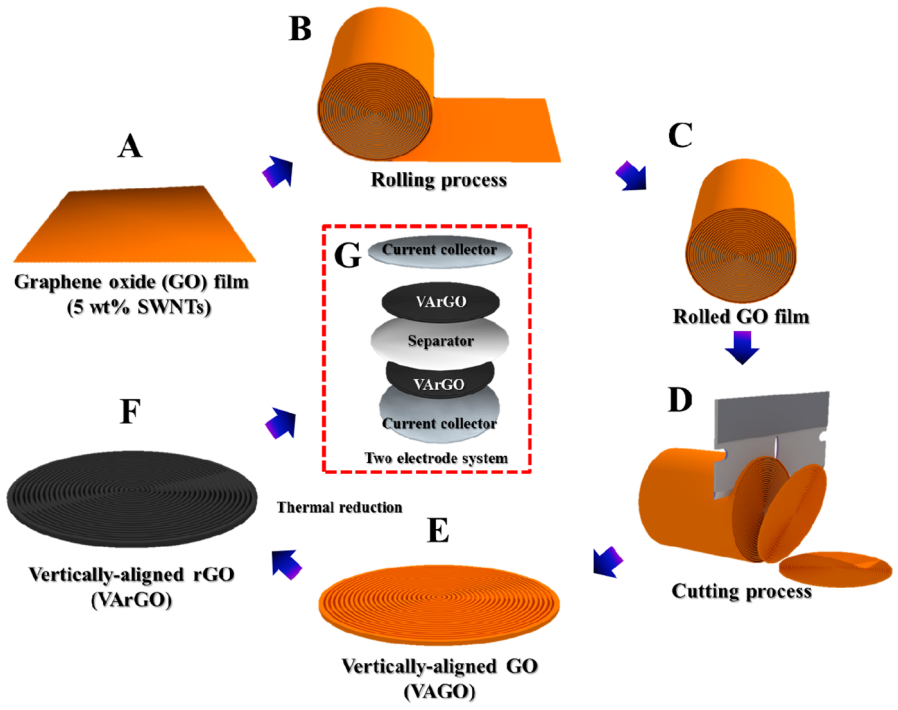

Scheme 1. Schematic illustration of the fabrication of vertically-aligned reduced graphene oxide (VArGO) electrodes. (A) Ethanol was sprayed onto dried GO film and then left to stand for 5 min to allow ethanol to percolate into the surface of GO film. (B,C) Rolling process of GO film and rolled GO film. (D) The rolled GO film was cut into pieces across the cross-section by using a cryomicrotome under frozen temperature. Surprisingly, the cut-rolled pieces of the horizontally-rolled GO film were changed into the vertically-aligned GO film. (E,F) The vertically aligned cut-rolled GO film (VAGO) was reduced by a thermal reduction process to give VArGO film. (G) As-prepared VArGO was used as an electrode without any other binder.

back to graphite by adding the SWCNTs as a spacer.[25,30] Those XRD results have produced very similar results with chemically bonded graphene/CNT composites.[25] In order to clearly determine the role of SWCNTs in the VArGO sheets, the porosity of VArGO was also measured with method of Brunaure–Emmett–Teller (BET) and Barrett–Joyner–Halenda (BJH). From the BET results, VArGO with SWCNTs indicated surface area of 123.78 m^2 g^{-1}; however, powder type of rGO and thick rGO film (270 μm) showed higher surface area (311.05 and 128.54 m^2 g^{-1}, respectively). Nevertheless, mesopore volume of VArGO (with SWCNTs (96.4%) and without SWCNTs (99.3%)) is much higher than those of thick rGO film (80.9%) and powder type of rGO (85.3%) (Figure S4, Supporting Information). The reduction of the mesopore volume in materials indicates that thermal expansion process for reduction of thick film of GO (see Figure S5, Supporting Information) may induce an increase of a macropore volume, resulting in the reduction of packing density of rGO materials. Furthermore, an existence of SWCNTs in VArGO affects a pore distribution of the VArGO film. To clearly identify a role of SWCNTs in the pore distribution of VArGO, we showed MP-plot of VArGO with and without SWCNTs in inset of Figure S4A,B (Supporting Information). According to those results, VArGO without SWCNTs showed that the micropore distribution is nearly closed to 0.4 nm (Figure S4B, Supporting Information), which is a similar result to the highly reduced GO;[31] however, that of VArGO with SWCNTs was shifted to nearly 0.9 nm (Figure S4A, Supporting Information). Therefore, we can clearly determine that SWCNTs can successfully act as a spacer for suitable pore size and conductive additive materials to improve conductivity and capacitance.[25,32] All materials are prepared as below. Before making GO film, the GO solution was mixed with a tiny amount of water-dispersible oxidized SWCNTs as an additive to control the pore size in VArGO (details in the Experimental Section). For comparison with other rGO electrodes made from powder or film, rGO_{Powder} and rGO_{Film} were carefully fabricated using the same composition. To make porous rGO samples, different heating rates were applied. Usually, rapid heating up to 130 °C (heating rate >5 °C/min) induces an explosive reduction reaction, which can generate highly porous rGO_{Powder} from dried GO film.[33] Although the surface area of rGO was greatly enhanced by fast heating, a polymer binder had to be used to coat the current collector, and it was hard to achieve a high packing density, as shown in Figure S5 and Table S1 (Supporting Information). To prepare horizontally stacked rGO film, a slow heating rate (heating rate <0.2 °C/min) was applied. When the film was reduced by a chemical reductant (N_2H_4), the resulting horizontally stacked GO film had large pores, but a low packing density[34] (Figures S5 and S6E, Supporting Information). In contrast, VArGO reduced thermally from GO starting

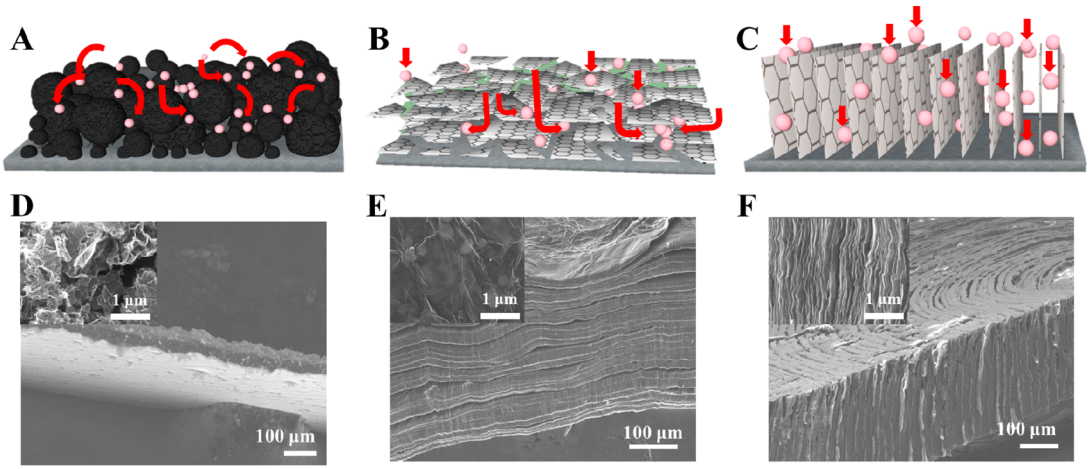

Figure 1. Schematic illustration of ion diffusion direction based on the morphologies of three rGO electrodes (rGO_{Powder}, rGO_{Film}, and VArGO). (A) Electrolyte ions were inhomogeneously entered into the different types of surface morphologies of rGO_{Powder} sheets. (B) Electrolyte ions were hard to enter because of the too close stacking of the horizontally aligned rGO_{Film}. (C) Electrolyte ions were homogeneously and directly diffused into the vertically aligned rGO (VArGO) sheets. (D,E,F) Cross-sectional morphologies with the inset images of rGO_{Powder}, rGO_{Film}, and VArGO electrodes, respectively.

at a low temperature and increasing the temperature up to 1000 °C under an Ar atmosphere yielded VArGO film that could be used directly as an electrode material without any type of binder (Scheme 1).

To obtain a volumetric capacitor with a high packing density, capacitor performance, including fast ion diffusion of the electrolyte, was investigated for three different rGO electrodes (Table S1, Supporting Information). A schematic illustration of the direction of ion diffusion of the electrolytes for rGO_{Powder}, rGO_{Film}, and VArGO are shown in Figure 1. We illustrated that the diffusion directions of the electrolyte ions would differ among these materials on the basis of the stacked shapes of 2D rGO sheets as described in ref 35. The morphologies and nanostructures of the three samples were characterized by scanning electron microscopy (SEM), as shown Figure 1. rGO_{Powder} was coated onto a current collector with 10% polyvinylidene flouride (PVDF) as a binder. Although coating of rGO onto the current collector with controllable thickness was simple, there were numerous micrometer-scale vacancies in the coated rGO electrode, which resulted in a low packing density (Figure 1A,D and inset).[21] The electrolyte ions should be inhomogeneously entered into the different types of surface morphologies of rGO_{Powder} sheets. On the other hand, rGO_{Film} had a horizontally stacked rGO structure, and could be used directly as an electrode without binder. However, the interlayer distance between the basal plane of the rGO layers was too close to diffuse electrolyte ions, leading to limited ion accessibility. Furthermore, as two 2D rGO sheets were combined into one rGO and the area of the combined 2D rGOs increased, the ion diffusion length of the electrolyte ions to the current collector increased sharply, resulting in slow charge/discharge rates (Figure 1B,E). In the case of VArGO, SEM revealed vertically aligned rGO films with an opened-edge structure (Figure 1C,F). Surprisingly, the opened-edge structures were not crushed by cutting (inset of Figures 1F and S5, Supporting Information), most likely because the films were cut after deep-freezing. Further thermal reduction of VArGO at a heating rate of 0.14 °C/min (5 °C/min for rGO_{Powder}) up to 1000 °C for 1 h removed most oxygen functional groups of GO to give highly conductive rGOs,[12,36] which was confirmed by X-ray photoelectron spectroscopy (XPS) and elemental analysis (EA) (Figure S7, Supporting Information). Full survey XPS spectra of VArGO were shown in Figure S7A (Supporting Information). From XPS, VArGO thermally reduced at 1000 °C does not contain any impurities (Carbon: 97.28% and Oxygen: 2.71%). As matter of fact, the elemental composition of XPS is very similar to that of EA (Cabon: 95.24%, Hydrogen: 0.25%, and Oxygen: below 4%). Therefore, we can conclude that the packing density of VArGO was not affected by any other impurities. Interestingly, there was a big difference in conductivity between rGO_{Powder} and VArGO (rGO_{Film}), even though their chemical composition is similar, since the chemical structures of rGOs was obtained under the same reduction conditions (1000 °C for 1 h). We concluded that the homogeneous stacking and denser nature of the rGO films *versus* the rGO powder resulted in better-aligned networks between rGO sheets (Table S1, Supporting Information). As a result, the conductance of VArGO (rGO_{Film}) was higher than that of rGO_{Powder}.[37]

As mentioned earlier, because liquid electrolyte ions can only diffuse through interlayer gaps and pores, different rGO shapes are likely to have different ion accessibilities, diffusion lengths, and diffusion paths of the electrolyte ions, which are important factors that determine the charge/discharge rate of a supercapacitor. We identified that the interlayer distances

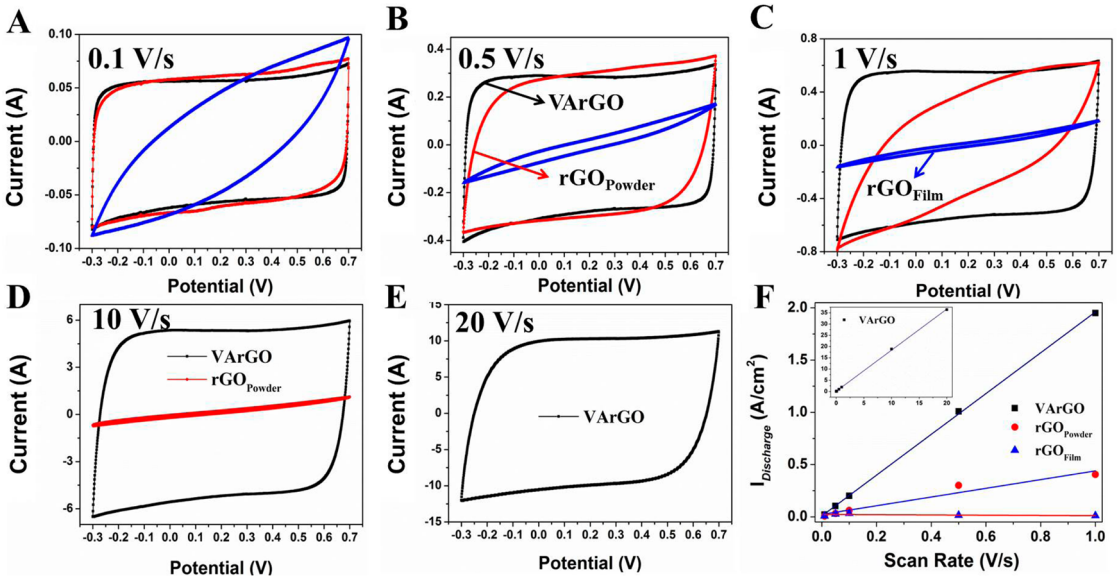

Figure 2. Electrochemical characteristics of the three rGO_{Powder}, rGO_{Film}, and VArGO electrodes with 6.0 M KOH as the electrolyte. (A−D) As the scan rate increased from 0.1 to 10 V/s, the capacitive current density of rGO_{Powder} and rGO_{Film} materials decreased gradually. (A−E) CV curves of VArGO were rectangular, even at a scan rate of 20 V/s. (F) Discharge current densities as a function of scan rate. Amazingly, only VArGO film showed a linear relationship between current density and scan rate, even at a high scan rate.

between inner rGO_{Powder} sheets and outer rGO_{Powder} sheets were not homogeneous, resulting in a broad range of charge/discharge times. For rGO_{Film}, the interlayer distances were too narrow to allow electrolyte ions to move effectively, and horizontally closed rGO layers formed from the merger of two rGO layers into one rGO layer were characterized by increased ion diffusion lengths. However, we suggested that the ion diffusion length of vertically aligned, opened-edge, and highly homogeneous VArGO film would be the shortest among the three different rGO and translate into the fastest charge/discharge rate and the highest packing density among the three different rGOs. We also predicted that the ion diffusion length of vertically aligned rGOs would not increase even when two rGOs were combined into one rGO as predicted for horizontally aligned rGO_{Film}, because the number of rGOs that combined was expected to be much less than that of rGO_{Film} because of lack of strong interactions between homogeneously aligned VArGOs and the substrate, and no gravity effect. Therefore, we demonstrated that relative to the other two rGO types, VArGO film would have the highest capacitance and best electrochemical reactivity due to large amount of homogeneously adsorbed/desorbed electrolyte ions and a high charge/discharge rate.

We used a two-electrode system to characterize the electrochemical characteristics of the as-fabricated VArGO in comparison with other electrodes according to scan rate. CV results for rGO_{Film}, rGO_{Powder}, and VArGO in 6.0 M KOH electrolyte at scan rates of 0.1, 0.5, 1, 10, and 20 V/s are shown in Figure 2A−E. Both rGO_{Powder} and rGO_{Film} were hard coated onto the current collector to obtain an equivalent current and thickness to that of VArGO (Table S1, Supporting Information). Current of rGO_{Powder} and VArGO increased sharply in comparison with that of rGO_{Film} at a scan rate of 0.1 V/s. In addition, the CV curve of VArGO was the most rectangular at increased scan rates, and its integrated area was largest. Furthermore, the rectangular scan shape obtained for VArGO was maintained across all voltage ranges from −0.3 to 0.7 V up to 20 V/s, indicating that VArGO has ideal electrochemical properties for charging/discharging processes. In contrast, the current of rGO_{Powder} and rGO_{Film} decreased significantly as the scan rate increased, as shown in the Figure 2F. Current of rGO_{Film} and rGO_{Powder} were almost straight lines at a scan rate of 1 V/s (Figure 2C) and 10 V/s (Figure 2D), respectively, indicating that at high scan rates, charging/discharging of rGO_{Film} and rGO_{Powder} did not occur because of limited ion mobility. Relationship between current (extracted from the current density of the electrode at 0.2 V for the CV profile of the discharge curve) and the applied scan rate is shown in Figure 2F. Surprisingly, the evolved discharge current of the VArGO electrode had an almost linear relationship with scan rate in the voltage range from 0.1 to 20 V/s. A linear relationship with $R^2 = 0.9996$ was observed for the discharging curves, indicating that the charging/discharging process was remarkably fast over the entire electrode surface, even at a high scan rate,[38] while the current of rGO_{Powder} and rGO_{Film} did not exhibit a linear dependence, even at the very low scan rates of 0.1 and 0.5 V/s, respectively ($R^2 = 0.9328$ and −0.0878). A linear relationship was only observed at very slow scan rates (0.01−0.1 V/s),

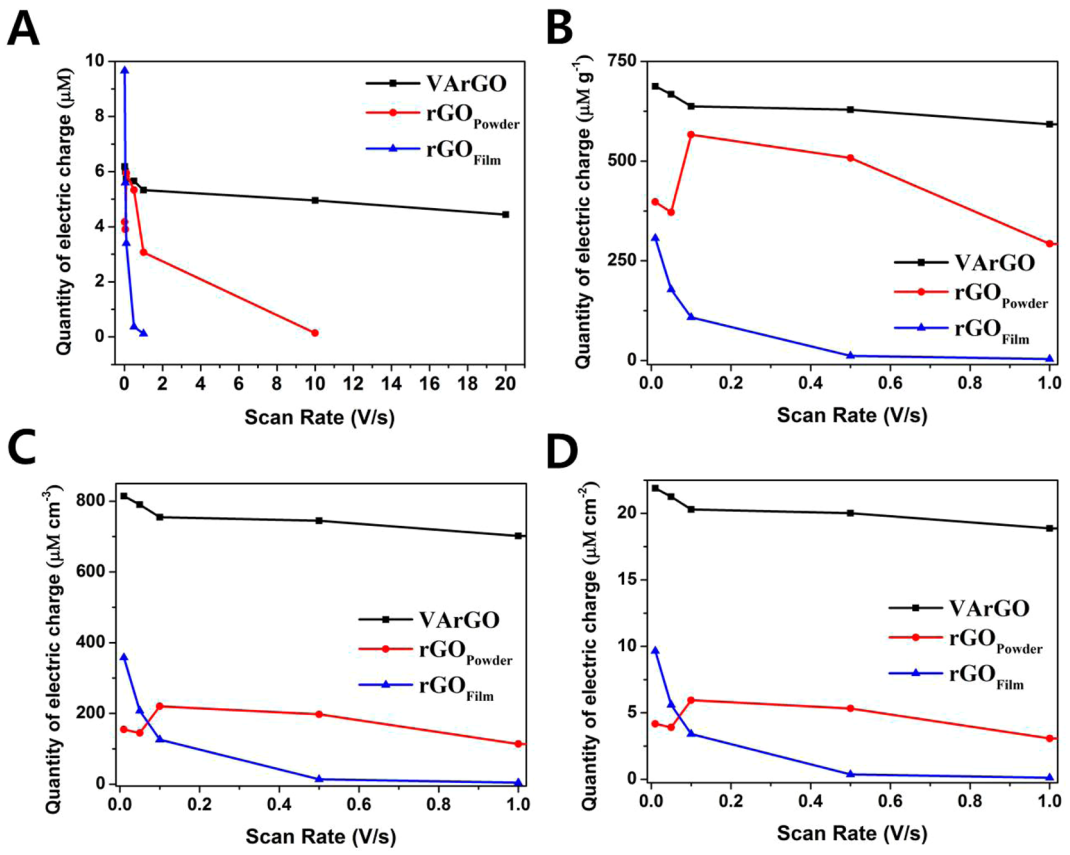

Figure 3. Volumetric and areal electrochemical characteristics of three rGO_{Powder}, rGO_{Film}, and VArGO electrodes. (A) The quantity of electric charges of overall electrodes (μM). (B–D) Gravimetric ($\mu M\ g^{-1}$), volumetric ($\mu M\ cm^{-3}$), and areal ($\mu M\ cm^{-2}$) quantity of electric charges of three electrodes. The VArGO electrode showed the highest gravimetric, volumetric, and areal quantity of electric charges.

indicating poor performance due to inhomogeneous porosity, a closely stacked surface, and/or the long ion diffusion length of rGO_{Powder} and rGO_{Film} electrodes.[35,38] In comparison with other rGO_{Powder} and rGO_{Film} electrodes, this ultrahigh capability of VArGO electrodes underscores the enhanced power performance.[2,38]

Performance of carbon-based electrodes in supercapacitors is highly dependent on the effective area of surface, mass, volume, and electrical conductance properties of the electrode materials.[6,14,39,40] However, existing porous electrodes for batteries and supercapacitors have often failed to live up to claims of exceptional performance when applied to an entire device system with limited space.[20,21] For a commercial supercapacitor product, high packing density and effective reacting surface area in a limited space is required, thus necessitating the introduction of the concept of a shape-engineered electrode with high packing density for volumetric capacitor. To further characterize the electrochemical performance of the VArGO electrodes, we have demonstrated quantity of electric charge at discharge curve from CV results (Figure 3). The overall quantity of the electric charge in the three electrodes are described in Figure 3A. As we expected, VArGO electrodes showed a uniform trend even increasing the scan rate, even though their initial quantity of electric charge is smaller than that of rGO_{Film} electrodes. To know the effective reacting mass ($\mu M\ g^{-1}$), volume ($\mu M\ cm^{-3}$), and surface ($\mu M\ cm^{-2}$) of electrodes, each unit was converted (details in the Experimental Section). The volumetric quantity of electric charge of the highly compacted VArGO electrode (814.5 $\mu M\ cm^{-3}$) was nearly 5.3-fold higher than that of rGO_{Powder} (154.6 $\mu M\ cm^{-3}$) and 2.3-fold higher than that of rGO_{Film} (357.0 $\mu M\ cm^{-3}$) at scan rate of 0.1 V/s (Figures 3C and S12B, Supporting Information). Although rGO_{Film} showed higher value than that of VArGO electrodes at initial stage, its quantity of electric charge was significantly reduced as the scan rate increased since horizontally closed-stacked structure induced to increase the passing resistance of electrolyte even though their high packing density induced good volumetric performance. Therefore, rGO_{Powder} showed a nonuniform trend as the scan rate increased because of inhomogeneity of electrode surface. Furthermore, the areal quantity of electric charge of the VArGO electrode (21.90 $\mu M\ cm^{-2}$) was 5.25-fold higher than that of rGO_{Powder} (4.17 $\mu M\ cm^{-2}$) and 2.26-fold higher than that of rGO_{Film} (9.66 $\mu M\ cm^{-2}$), indicating that the opened-edge and vertically aligned rGO structure had high reactivity due to good diffusion

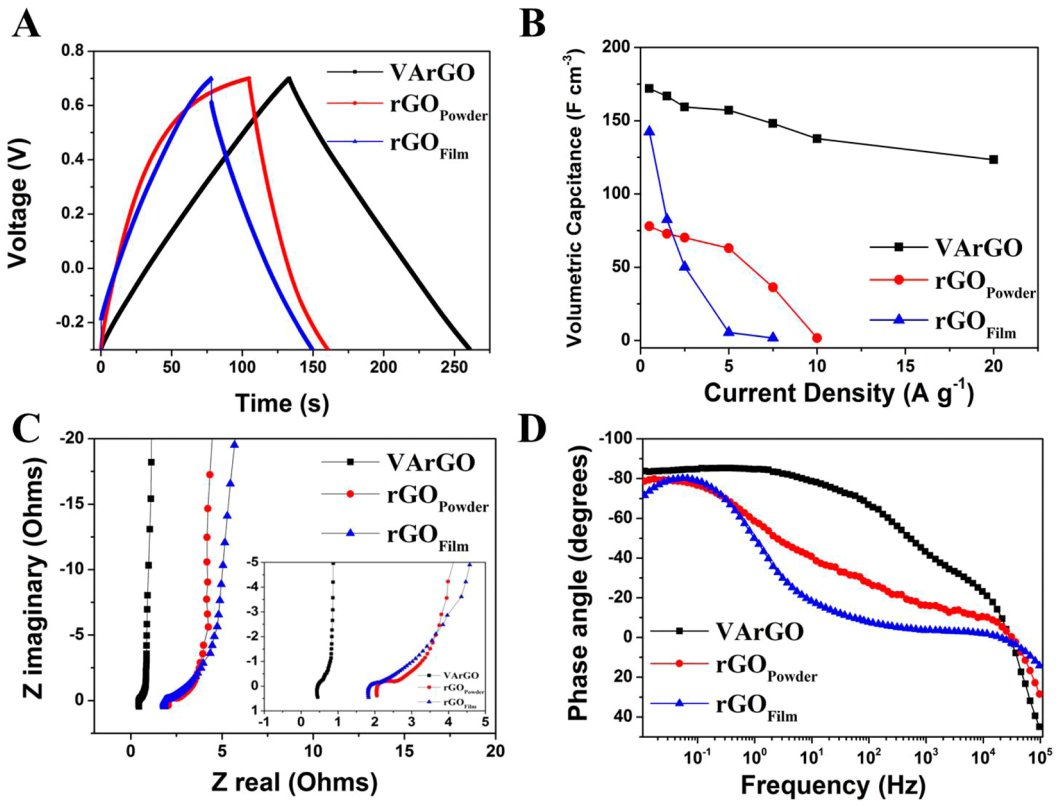

Figure 4. Supercapacitor performances of three rGO_{Powder}, rGO_{Film}, and VArGO electrodes in ECs with 6.0 M KOH electrolyte. (A) Galvanostatic charge/discharge curves at a current density of 0.5 A g^{-1}. (B) Dependence of volumetric capacitance on the current density. (C) Nyquist plots with inset of high frequency region. (D) Bode plots of phase angle *versus* frequency.

of electrolyte ions and electrochemical behavior (Figures 3D and S12C, Supporting Information). These results are similar to those reported for edge graphene and edge graphite in comparison with basal plane of them.[41−43]

Because the shape of engineered electrode materials can affect their electrochemical properties, we carefully studied the supercapacitor performance of rGO_{Powder}, rGO_{Film}, and VArGO film electrodes. supercapacitor performance was investigated using a symmetrical two-electrode system in 6.0 M KOH electrolyte (Figure 4). Galvanostatic charge/discharge curves of the VArGO double-layer capacitor in 6.0 M KOH electrolyte were observed at a current density of 0.5 A/g (Figure 4A). rGO_{Powder} had a gradual charge curve relative to the discharge curve. Even though soft loading of rGO_{Powder} onto the current collector resulted in a capacitor with symmetric charging/discharging characteristics, the charge/discharge curves became asymmetric as the loading amount increased (Figures 4A, S8C,D, Supporting Information). In addition, the charge/discharge curves of rGO_{Film} were small and showed a similar behavior to that of rGO_{Powder} with a significant IR drop at the same current density, in contrast to the symmetric curves of VArGO that did not change (Figures 4A, S8A,B, Supporting Information). Charging curves of the VArGO electrode were almost symmetric with respect to the discharging curves within the potential ranges of 0.3−0.7 V without an IR drop, indicating that the capacitive reversibility of the VArGO electrode was high, consistent with its electrochemical characteristics. We demonstrated that the opened-edge and vertically aligned rGO film structure had a positive influence on electrochemical performance even at high loading amounts and increased film thicknesses (Figures S8 and S11, Supporting Information).

VArGO electrode had a gravimetric capacitance of up to 145 ± 1 F g^{-1} at a current density of 0.5 A/g, which was lower than that of rGO_{Powder} (159 ± 1 F g^{-1}). However, when gravimetric capacitance was converted to volumetric capacitance, VArGO electrode had much higher capacitance (171 ± 1 F cm^{-3}) than rGO_{Powder} (62 ± 1 F cm^{-3}), as shown in Figure 4B. Surprisingly, the volumetric capacitance of VArGO only decreased to 123 ± 1 F cm^{-3} at a current density of 20 A/g, while the rGO_{Powder} had a capacitance of only 1 ± 1 F cm^{-3} at the current density of 10 A/g, suggesting that the VArGO supercapacitor had high rate capability. Furthermore, rGO_{Film} had a volumetric capacitance of 142 ± 1 F cm^{-3}, but its capacitance decreased significantly to 2 ± 1F cm^{-3} at a current density of 7.5 A/g. In addition, the volumetric capacitances of all rGO electrodes decreased as the film thickness of the electrode increased (Figure S8, Supporting Information). As expected, as film thickness

increased, current density also increased.[21] The volumetric and areal capacitances of the VArGO electrode decreased from 171 ± 1 F cm^{-3} and 1.83 ± 0.01 F cm^{-2} to 153 ± 1 F cm^{-3} and 1.44 ± 0.01 F cm^{-2}, respectively, as the thickness of the electrode increased from 270 to 370 μm (Figure S13A,B, Supporting Information). Although the volumetric and areal capacitances of rGO$_{Powder}$ at the initial current density were 66 ± 1 F cm^{-3} and 0.19 ± 0.01 F cm^{-2} at 90 μm and 62 ± 1 F cm^{-3} and 0.06 ± 0.01 F cm^{-2} at 270 μm, respectively (Figure S13C,D, Supporting Information), these values decreased drastically at a current density of 5 A/g (Figure S14, Supporting Information). Volumetric and areal capacitances of rGO$_{Film}$ were 195 ± 1 F cm^{-3} and 0.78 ± 0.01 F cm^{-2} at 30 μm and 142 ± 1 F cm^{-3} and 0.60 ± 0.01 F cm^{-2}, respectively (Figure S13C,D, Supporting Information). These values are higher than those measured for VArGO and rGO$_{Powder}$ electrodes at the initial stage, but these values decreased significantly as the thickness of the rGO$_{Film}$ increased (Figure S13C,D, Supporting Information). As a result, the VArGO electrode showed a much better ion transportation rate in EC cells than the other rGO electrodes. Furthermore, the VArGO electrode was stable at a current density of 20 A/g for over 15 000 cycles, as shown in Figure S14 (Supporting Information). After 15 000 cycles, the capacitance of the VArGO electrode reached 94.8% of its initial capacitance. Therefore, VArGO electrode had a high energy density of 7.43 W h L^{-1} at 209.58 W L^{-1}, which decreased gradually to 6.51 W h L^{-1} at 2.05 KW L^{-1}. This value is much higher than the corresponding rGO$_{Powder}$ and rGO$_{Film}$ electrode values (Figure S16, Supporting Information). Meanwhile, the VArGO electrode displayed effective electrochemical energy and power densities.

We next investigated the kinetic features of ion diffusion in the electrodes using electrochemical impedance spectroscopy (EIS) in an aqueous electrolyte system. A Nyquist plot obtained for a two-electrode double-layer capacitor cell constructed with both electrodes in 6.0 M KOH in the frequency range from 100 kHz to 0.01 Hz is shown in Figure 4C. The inset of Figure 4C is a magnified view of the high-frequency range. Nyquist plot for the double-layer capacitor was characterized by a high frequency semicircle caused by its effective series resistance, which we attributed to ionic conductivity between the electrode materials and electrolyte. The nonperfectly formed semicircle of VArGO in the high frequency region of the Nyquist plot implied the existence of high ionic conductivity at the interface of the electrodes and electrolyte, consistent with the high scan rate capability and lack of porous electrode characteristics of the VArGO electrode.[38] With the best ion response, VArGO showed the lowest resistance (R_s = 0.44 Ω) in comparison with the rGO$_{Powder}$ (2.05 Ω) and rGO$_{Film}$ (1.82 Ω) electrodes. The slope of VArGO in comparison with those of the curves of the other rGO electrodes was nearly vertical even in the low frequency region, indicating that the vertically aligned and opened-edge structured VArGO electrode had the best ion diffusion behavior of the three electrode types evaluated. The dependence of the phase angle on frequency (Bode phase plot) for rGO$_{Powder}$, rGO$_{Film}$, and VArGO is shown in Figure 4D. For frequencies up to 6.6 Hz, the phase angle of VArGO was close to −85.3°, suggesting that the performance of the device was almost the same as that of an ideal capacitor.[7,21] The characteristic frequency, f_0, for a phase angle of −45° was 810.5 Hz. This frequency marked the point at which the resistive and capacitive impedances were equal. The corresponding time constant τ_0 (= 1/f_0) equaled 1 ms, compared with 222 ms (4.5 Hz at −45°) for the rGO$_{Powder}$ and 909 ms (1.1 Hz at −45°) for the rGO$_{Film}$. This rapid frequency response of VArGO was made possible by the accessible pore structure of VArGO; the vertically aligned and opened-edge structure enhanced the electrolyte ion transport rate in the EC cell. The VArGO electrode dealt with in this work showed improved electrochemical reactivity, volumetric capacitance and more dense electrodes in comparison to other carbon-based electrode materials. For example, graphene form and graphene hydrogel showed very low volumetric capacitance of 1−4 F cm^{-3} due to their low packing density of 0.01−0.03 g cm^{-3}, even though they showed high gravimetric capacitance.[13] Laser-scribed graphene film also shows a very low density of 0.06 g cm^{-3}, which is induced low volumetric capacitance of 12.1 F cm^{-3} because of large pore volume.[21] High density graphene-based electrodes were developed such as partially reduced GO paper[44] and compressed activated microwave-expanded graphite oxide (a-MEGO),[26] exhibiting modest volumetric capacitance 95 F cm^{-3} at 0.46 g cm^{-3} and 110 F cm^{-3} at 0.75 g cm^{-3} (uncompressed 54 F cm^{-3} at 0.34 g cm^{-3}), respectively. Since their packing densities were still lower than 1 g cm^{-3}, it is really necessary to have a high packing density with suitable electrode's shape for improving performance of electrode in compact supercapacitor. The VArGO electrodes with SWCNTs as a spacer indicated in this work achieves the large volumetric capacitance (171 F cm^{-3}) with high packing density electrode and easy fabrication method for making a vertically aligned shape used herein. It should be also noted that the density of this graphene composite is more than 3 fold higher than that of activated carbon (0.5 g cm^{-3}), which is the dominant materials used in supercapacitor electrodes.

CONCLUSIONS

In conclusion, vertically aligned and opened-edge VArGO electrodes with a high packing density of 1.18 g cm^{-3} were easily prepared using simple rolling and cutting processes. As-prepared VArGO electrodes

with appropriate interlayer distances and pores showed the highest volumetric and areal electrochemical characteristics in comparison with rGO_{Powder} and rGO_{film} electrodes. Furthermore, the vertically aligned structure of the VArGO electrode yielded the highest electrolyte ion diffusion in the cell, leading to a great improvement in electrochemical characteristics to a degree suitable for supercapacitor applications. Surprisingly, enhanced electrochemical characteristics were maintained even as the film thickness increased, which we attributed to the vertical rGO film structure. We obtained a very high volumetric capacitance of 171 F cm^{-3} and areal capacitance of 1.83 F cm^{-2} for the VArGO electrode in 6.0 M KOH electrolyte. The high performance vertically aligned rGO electrode synthesized by a simple and facile process described in this work is ideal for application in compact energy storage applications.

EXPERIMENTAL SECTION

Synthesis of Graphene Oxide (GO). Water-dispersed single GO sheets were synthesized according to prior reports.[18] GO was prepared from natural graphite powder (Bay Carbon, SP-1 graphite) using the modified Hummers and Offenman's method with H_2SO_4, $NaNO_3$, and $KMnO_4$.

Oxidation of Single-Walled Carbon Nanotubes (SWCNTs). One hundred milligrams of SWCNTs (ILJIN Nanotech) were dispersed in 85 mL of a 3:1 mixture of H_2SO_4 (98 wt %) and HNO_3 (16 M). After 3 days of bath sonication, the oxidized SWCNT-acid mixture was diluted with 1 L of deionized water, stirred for an hour, and then vacuum filtered using 0.45-μm filter paper. The filtrant was washed with 1 L of deionized water again, stirred for an hour, and vacuum filtered again. These steps were repeated until all the acids had washed out. The last filtrant was washed with the smallest amount of deionized water, collected on an AAO membrane (Anodisk), and dried overnight.

Fabrication of GO Film. Before fabrication of GO film, 100 mg of oxidized SWCNTs were mixed with 2 mg mL^{-1} of GO dispersion by sonication and homogenization to obtain a homogeneous mixture. The GO/oxidized SWCNT dispersion was then transferred into a Petri dish with a diameter of 20 × 30 cm, and dried at room temperature overnight. After complete drying, it was easy to peel off the GO film from the Petri dish to characterize its chemical and structural properties.

Fabrication of rGO Film. rGO film was formed by thermal reduction at 1000 °C for 1 h (0.14 °C/min) under a argon atmosphere. This slow heating rate was used to prevent explosive reduction into rGO_{Powder}.

Fabrication of rGO Powder. As-fabricated GO solid (500 mg) was transferred into an alumina boat prior to placement in a furnace. Then, 220 mg of rGO powder was obtained by thermal reduction at 1000 °C for 1 h (heating rate above 5 °C/min) under a argon atmosphere (yield: 26%). Two different kinds of rGO materials were obtained with various heating rates. Film-type rGO material was generated by slow heating (0.14 °C/min), while powder-type rGO material was produced by fast heating (5 °C/min), since many oxygen groups on rGO sheets escaped during thermal reduction at temperatures below 150 °C.

Fabrication of Vertically Aligned Reduced Graphene Oxide (VArGO). Surface of as-fabricated GO film was slightly wetted with ethanol to allow it to be tightly rolled. Before drying, it was frozen at −40 °C and then placed in a rotary cryomicrotome, which is used in the biomaterials laboratory to cut specimen into thin pieces confirmed with SEM or TEM. By using the rotary cryomicrotome, we could control the thickness of rGO films in a less than 10 μm. The cut sections were fully dried in a vacuum oven, followed by thermal annealing at temperatures up to 1000 °C for 1 h (0.14 °C/min) to obtain VArGO film that was used directly as an electrode.

Characterization of Materials. Microstructural characterizations were performed using a JEOL JSM-7404F field emission scanning electron microscope (FE-SEM) operated at 15 kV. Chemical structure characterizations of rGO_{Powder}, rGO_{Film}, and VArGO were performed. XRD measurements were performed on a Rigaku Ultima IV X-ray diffractometer with Cu Kα radiation at a scanning rate of 5°/min. All XPS measurements were performed on a Thermo VG Microtech ESCA 2000 with a monochromatic Al Kα X-ray source at 100 W. Cutting was performed using a Lieca Biosystems CM3050 S at a low temperature (−40 °C).

Electrochemical Characterization. Prototype supercapacitors with 6.0 M KOH electrolyte and rGO_{Powder}, rGO_{Film}, or VArGO as electrodes were assembled in a symmetrical two-electrode configuration using a previously reported procedure.[14,39] The prototype supercapacitor cell consisted of two current collectors (Ni foil, Sigma-Aldrich), two electrodes (active materials), and an ion porous separator (Whatman filter paper) supported in a test fixture consisting of two glasses as the antistatic material. rGO_{Film} and VArGO did not require binder materials. However, to prepare rGO_{Powder} electrodes, rGO_{Powder} was dispersed in 10 times weighted *N*-methyl-2-pyrrolidone (NMP, Sigma-Aldrich) and then 10 wt % polyvinylidene fluoride (PVDF, Sigma-Aldrich) was added to rGO_{Powder} as a binder. rGO_{Powder} and PVDF were mixed into a slurry using a ball-mill (200 rpm, 6 h). The well-mixed slurry was stirred for 24 h at room temperature to obtain homogeneous slurry. The as−prepared rGO_{Powder} slurry was coated onto the end of Ni foil (1 cm × 1 cm on a 1 cm × 3 cm piece of Ni foil). A pair of typical electrodes had a weight of around 3.5 mg (thickness of 90 μm) and 10.5 mg (thickness of 270 μm) after drying overnight at ∼80 °C under a vacuum. They were then pressed at a pressure of 15 MPa. Prototype cells with two symmetrical rGO_{Powder} electrodes were assembled in atmosphere. Assembled cells were wrapped with Teflon and then infiltrated with 6.0 M KOH solution as the electrolyte. Cyclic voltammetry and galvanostatic charge/discharge measurements of all cells were obtained over the potential range of −0.3 to 0.7 V, while electrochemical impedance spectroscopy was performed between 100 kHz and 0.01 Hz. All tests were performed using a CHI660D electrochemical workstation. Quantity of electric charge values was calculated from integrated discharge current in CV results using the following formula:

$$\text{quantity of electric charge } (M) = A(V/V/s)/96485$$

where A is the current density, V is the voltage, and V/s is the scan rate. Gravimetric, volumetric, and areal capacitance values were calculated from galvanostatic charge/discharge curves using the following formula:

$$C = It/m\Delta V$$

where I is the constant current, m is the total mass of both graphene electrodes (gravimetric), total volume of both graphene electrodes (volumetric), or total area of both graphene electrodes (areal), and dV/dt was calculated from the slope obtained by fitting a straight line to the discharge curve over the range of V_{max} (voltage at the beginning of discharge) to 1/2 V_{max}.

Energy density and power density of the electrodes were calculated using the following equation:

$$E = \frac{1}{8} \times C(\Delta V)^2$$

$$P = E/t$$

where C is the specific volumetric capacitance of the electrode, ΔV is the potential range, P is the power density, and t is the time to discharge.

Conflict of Interest: The authors declare no competing financial interest.

Acknowledgment. This work was supported by the National Research Foundation of Korea (NRF) grant funded by the Korean government (MSIP) (Grant No. 2006-0050684) and partially by ISTK (Grant B551179-13-01-01).

Supporting Information Available: (1) Cutting process of VArGO using microtome at location in Figure S1. (2) Characterization of materials by digital camera, XRD, SEM and XPS. (3) Further electrochemical characteristics for electrode materials. This material in available free of charge *via* the Internet at http://pubs.acs.org.

REFERENCES AND NOTES

1. Eigler, S.; Enzelberger-Heim, M.; Grimm, S.; Hofmann, P.; Kroener, W.; Geworski, A.; Dotzer, C.; Röckert, M.; Xiao, J.; Papp, C.; *et al.* Wet Chemical Synthesis of Graphene. *Adv. Mater.* **2013**, *25*, 3583–3587.
2. Pech, D.; Brunet, M.; Durou, H.; Huang, P.; Mochalin, V.; Gogotsi, Y.; Taberna, P.-L.; Simon, P. Ultrahigh-Power Micrometre-Sized Supercapacitors Based on Onion-Like Carbon. *Nat. Nanotechnol.* **2010**, *5*, 651–654.
3. Simon, P.; Gogotsi, Y. Materials for Electrochemical Capacitors. *Nat. Mater.* **2008**, *7*, 845–854.
4. Miller, J. R.; Outlaw, R. A.; Holloway, B. C. Graphene Electric Double Layer Capacitor with Ultra-High-Power Performance. *Electrochim. Acta* **2011**, *56*, 10443–10449.
5. Stoller, M. D.; Park, S.; Zhu, Y.; An, J.; Ruoff, R. S. Graphene-Based Ultracapacitors. *Nano Lett.* **2008**, *8*, 3498–3502.
6. Zhu, Y.; Murali, S.; Stoller, M. D.; Ganesh, K. J.; Cai, W.; Ferreira, P. J.; Pirkle, A.; Wallace, R. M.; Cychosz, K. A.; Thommes, M.; *et al.* Carbon-Based Supercapacitors Produced by Activation of Graphene. *Science* **2011**, *332*, 1537–1541.
7. El-Kady, M. F.; Strong, V.; Dubin, S.; Kaner, R. B. Laser Scribing of High-Performance and Flexible Graphene-Based Electrochemical Capacitors. *Science* **2012**, *335*, 1326–1330.
8. Liu, F.; Song, S.; Xue, D.; Zhang, H. Folded Structured Graphene Paper for High Performance Electrode Materials. *Adv. Mater.* **2012**, *24*, 1089–1094.
9. Xiao, X.; Liu, P.; Wang, J. S.; Verbrugge, M. W.; Balogh, M. P. Vertically Aligned Graphene Electrode for Lithium Ion Battery with High Rate Capability. *Electrochem. Commun.* **2011**, *13*, 209–212.
10. Lee, S. W.; Yabuuchi, N.; Gallant, B. M.; Chen, S.; Kim, B.-S.; Hammond, P. T.; Shao-Horn, Y. High-Power Lithium Batteries from Functionalized Carbon-Nanotube Electrodes. *Nat. Nanotechnol.* **2010**, *5*, 531–537.
11. Miller, J. R.; Outlaw, R. A.; Holloway, B. C. Graphene Double-Layer Capacitor with Ac Line-Filtering Performance. *Science* **2010**, *329*, 1637–1639.
12. Yoon, Y.; Seo, S.; Kim, G.; Lee, H. Atomic Dopants Involved in the Structural Evolution of Thermally Graphitized Graphene. *Chem. Eur. J.* **2012**, *18*, 13466–13472.
13. Zhang, X.; Sui, Z.; Xu, B.; Yue, S.; Luo, Y.; Zhan, W.; Liu, B. Mechanically Strong and Highly Conductive Graphene Aerogel and Its Use as Electrodes for Electrochemical Power Sources. *J. Mater. Chem.* **2011**, *21*, 6494–6497.
14. Yoon, Y.; Lee, K.; Baik, C.; Yoo, H.; Min, M.; Park, Y.; Lee, S. M.; Lee, H. Anti-Solvent Derived Non-Stacked Reduced Graphene Oxide for High Performance Supercapacitors. *Adv. Mater.* **2013**, *25*, 4437–4444.
15. Murali, S.; Dreyer, D. R.; Valle-Vigon, P.; Stoller, M. D.; Zhu, Y.; Morales, C.; Fuertes, A. B.; Bielawski, C. W.; Ruoff, R. S. Mesoporous Carbon Capsules as Electrode Materials in Electrochemical Double Layer Capacitors. *Phys. Chem. Chem. Phys.* **2011**, *13*, 2652–2655.
16. Biswas, S.; Drzal, L. T. Multilayered Nanoarchitecture of Graphene Nanosheets and Polypyrrole Nanowires for High Performance Supercapacitor Electrodes. *Chem. Mater.* **2010**, *22*, 5667–5671.
17. Kim, T. Y.; Lee, H. W.; Stoller, M.; Dreyer, D. R.; Bielawski, C. W.; Ruoff, R. S.; Suh, K. S. High-Performance Supercapacitors Based on Poly(Ionic Liquid)-Modified Graphene Electrodes. *ACS Nano* **2010**, *5*, 436–442.
18. Moon, I. K.; Lee, J.; Ruoff, R. S.; Lee, H. Reduced Graphene Oxide by Chemical Graphitization. *Nat. Commun.* **2010**, *1*, 73.
19. Paredes, J. I.; Villar-Rodil, S.; Martínez-Alonso, A.; Tascón, J. M. D. Graphene Oxide Dispersions in Organic Solvents. *Langmuir* **2008**, *24*, 10560–10564.
20. Gogotsi, Y.; Simon, P. True Performance Metrics in Electrochemical Energy Storage. *Science* **2011**, *334*, 917–918.
21. Yang, X.; Cheng, C.; Wang, Y.; Qiu, L.; Li, D. Liquid-Mediated Dense Integration of Graphene Materials for Compact Capacitive Energy Storage. *Science* **2013**, *341*, 534–537.
22. Zhao, X.; Tian, H.; Zhu, M.; Tian, K.; Wang, J. J.; Kang, F.; Outlaw, R. A. Carbon Nanosheets as the Electrode Material in Supercapacitors. *J. Power Sources* **2009**, *194*, 1208–1212.
23. Bo, Z.; Zhu, W.; Ma, W.; Wen, Z.; Shuai, X.; Chen, J.; Yan, J.; Wang, Z.; Cen, K.; Feng, X. Vertically Oriented Graphene Bridging Active-Layer/Current-Collector Interface for Ultrahigh Rate Supercapacitors. *Adv. Mater.* **2013**, 5799–5806.
24. Futaba, D. N.; Hata, K.; Yamada, T.; Hiraoka, T.; Hayamizu, Y.; Kakudate, Y.; Tanaike, O.; Hatori, H.; Yumura, M.; Iijima, S. Shape-Engineerable and Highly Densely Packed Single-Walled Carbon Nanotubes and Their Application as Super-Capacitor Electrodes. *Nat. Mater.* **2006**, *5*, 987–994.
25. Jung, N.; Kwon, S.; Lee, D.; Yoon, D.-M.; Park, Y. M.; Benayad, A.; Choi, J.-Y.; Park, J. S. Synthesis of Chemically Bonded Graphene/Carbon Nanotube Composites and Their Application in Large Volumetric Capacitance Supercapacitors. *Adv. Mater.* **2013**, 6854–6858.
26. Murali, S.; Quarles, N.; Zhang, L. L.; Potts, J. R.; Tan, Z.; Lu, Y.; Zhu, Y.; Ruoff, R. S. Volumetric Capacitanceofcompressed Activatedmicrowave-Expandedgraphite Oxide (a-Mego)-Electrodes. *Nano Energy* **2013**, *2*, 764–768.
27. Chen, W.; Yan, L. Centimeter-Sized Dried Foam Films of Graphene: Preparation, Mechanical and Electronic Properties. *Adv. Mater.* **2012**, *24*, 6229–6233.
28. Seo, S.; Yoon, Y.; Lee, J.; Park, Y.; Lee, H. Nitrogen-Doped Partially Reduced Graphene Oxide Rewritable Nonvolatile Memory. *ACS Nano* **2013**, *7*, 3607–3615.
29. Fan, Z.; Yan, J.; Zhi, L.; Zhang, Q.; Wei, T.; Feng, J.; Zhang, M.; Qian, W.; Wei, F. A Three-Dimensional Carbon Nanotube/Graphene Sandwich and Its Application as Electrode in Supercapacitors. *Adv. Mater.* **2010**, *22*, 3723–3728.
30. Cheng, Q.; Tang, J.; Ma, J.; Zhang, H.; Shinya, N.; Qin, L.-C. Graphene and Carbon Nanotube Composite Electrodes for Supercapacitors with Ultra-High Energy Density. *Phys. Chem. Chem. Phys.* **2011**, *13*, 17615–17624.
31. Moon, I. K.; Lee, J.; Lee, H. Highly Qualified Reduced Graphene Oxides: The Best Chemical Reduction. *Chem. Commun.* **2011**, *47*, 9681–9683.
32. Wang, H.; Liu, Z.; Chen, X.; Han, P.; Dong, S.; Cui, G. Exfoliated Graphite Nanosheets/Carbon Nanotubes Hybrid Materials for Superior Performance Supercapacitors. *J. Solid State Electrochem.* **2011**, *15*, 1179–1184.
33. Yan, J.; Liu, J.; Fan, Z.; Wei, T.; Zhang, L. High-Performance Supercapacitor Electrodes Based on Highly Corrugated Graphene Sheets. *Carbon* **2012**, *50*, 2179–2188.
34. Niu, Z.; Chen, J.; Hng, H. H.; Ma, J.; Chen, X. A Leavening Strategy to Prepare Reduced Graphene Oxide Foams. *Adv. Mater.* **2012**, *24*, 4144–4150.
35. Bo, Z.; Wen, Z.; Kim, H.; Lu, G.; Yu, K.; Chen, J. One-Step Fabrication and Capacitive Behavior of Electrochemical Double Layer Capacitor Electrodes Using Vertically-Oriented Graphene Directly Grown on Metal. *Carbon* **2012**, *50*, 4379–4387.
36. Zhao, B.; Liu, P.; Jiang, Y.; Pan, D.; Tao, H.; Song, J.; Fang, T.; Xu, W. Supercapacitor Performances of Thermally Reduced Graphene Oxide. *J. Power Sources* **2012**, *198*, 423–427.
37. Jung, I.; Dikin, D. A.; Piner, R. D.; Ruoff, R. S. Tunable Electrical Conductivity of Individual Graphene Oxide

Sheets Reduced at "Low" Temperatures. *Nano Lett.* **2008**, *8*, 4283–4287.
38. Lin, J.; Zhang, C.; Yan, Z.; Zhu, Y.; Peng, Z.; Hauge, R. H.; Natelson, D.; Tour, J. M. 3-Dimensional Graphene Carbon Nanotube Carpet-Based Microsupercapacitors with High Electrochemical Performance. *Nano Lett.* **2012**, *13*, 72–78.
39. Yang, X.; Zhu, J.; Qiu, L.; Li, D. Bioinspired Effective Prevention of Restacking in Multilayered Graphene Films: Towards the Next Generation of High-Performance Supercapacitors. *Adv. Mater.* **2011**, *23*, 2833–2838.
40. Wen, Z.; Wang, X.; Mao, S.; Bo, Z.; Kim, H.; Cui, S.; Lu, G.; Feng, X.; Chen, J. Crumpled Nitrogen-Doped Graphene Nanosheets with Ultrahigh Pore Volume for High-Performance Supercapacitor. *Adv. Mater.* **2012**, *24*, 5610–5616.
41. Pandolfo, A. G.; Hollenkamp, A. F. Carbon Properties and Their Role in Supercapacitors. *J. Power Sources* **2006**, *157*, 11–27.
42. Yuan, W.; Zhou, Y.; Li, Y.; Li, C.; Peng, H.; Zhang, J.; Liu, Z.; Dai, L.; Shi, G. The Edge- and Basal-Plane-Specific Electrochemistry of a Single-Layer Graphene Sheet. *Sci. Rep.* **2013**, *3*, 2248.
43. Song, W.; Ji, X.; Deng, W.; Chen, Q.; Shen, C.; Banks, C. E. Graphene Ultracapacitors: Structural Impacts. *Phys. Chem. Chem. Phys.* **2013**, *15*, 4799–4803.
44. Hantel, M. M.; Kaspar, T.; Nesper, R.; Wokaun, A.; Kötz, R. Partially Reduced Graphene Oxide Paper: A Thin Film Electrode for Electrochemical Capacitors. *J. Electrochem. Soc.* **2013**, *160*, A747–A750.